U.P.B. Sci. Bull., Series C, Vol. 88, Iss. 3, 2026 ISSN 2286 – 3540

OPTIMIZING EFFICIENCY IN MULTI-STAGE RESONANT WPT BY CO-DESIGNING COIL INNER RADIUS AND TURN COUNT

Gang LIANG[1], Xin WANG[2], Chunlong LI*[3], Yongbo YAO[4], Qing LI[5]

For medium- and long-range contactless power delivery, multi-stage resonant magnetic wireless power transmission (WPT) is a compelling option; however, transmission efficiency remains the central hurdle to practical deployment. This paper aims to improve the efficiency of multi-stage magnetic resonant coupled WPT systems. Focusing on the critical geometric parameters that affect system efficiency, in-depth theoretical analysis, simulation studies, and experimental verification were conducted. An optimization method for key parameters of multi-stage magnetic resonant coupled WPT systems is proposed. Experimental results demonstrate that, after geometric parameter optimization, the system efficiency at a transmission distance of 900 mm is improved by approximately 16.9% compared with the non-optimized case.

Keywords: multi-stage magnetic resonance coupling; wireless power transfer; geometric parameter optimization; joint optimization

1. Introduction

Early explorations of contactless energy transmission appeared at the turn of the twentieth century and laid the groundwork for today's resonant wireless power transmission (WPT) [1]. It can be generally categorized into two types: radiative and non-radiative. The radiative type suffers from low transmission efficiency and is difficult to apply in practical scenarios. In contrast, non-radiative transmission is implemented mainly using electromagnetic induction and resonant coupling. Although it offers relatively high transmission efficiency, its effective transmission distance is usually limited to the centimeter-to-meter scale. WPT has

[1] Eng., State Grid Xinjiang Information & Telecommunication Company, State Grid Xinjiang Electric Power Co., Ltd, Urumqi, China
[2] Eng., State Grid Xinjiang Information & Telecommunication Company, State Grid Xinjiang Electric Power Co., Ltd, Urumqi, China, e-mail: wangxindfbc@163.com
* Corresponding author, e-mail: lcl198702@163.com
[3] Eng., China Electric Power Research Institute, Nanjing 210003, China
[4] Eng., State Grid Xinjiang Information & Telecommunication Company, State Grid Xinjiang Electric Power Co., Ltd, Urumqi, China
[5] Eng., State Grid Xinjiang Information & Telecommunication Company, State Grid Xinjiang Electric Power Co., Ltd, Urumqi, China

been widely applied in electronics, transportation, and power systems owing to its advantages in safety, reliability, and flexibility [2-5].

As smart grids have matured and scaled, WPT applications are increasingly targeting medium and long-range transmission. The efficiency of current long-distance WPT systems is influenced by multiple factors [6-8], For the traditional two-coil configuration, efficiency falls off quickly as the coil spacing approaches multiple coil dimensions. Existing studies have shown that adding multiple relay coils can effectively extend the transmission distance [9]. For example, Chen et al. at San Diego State University proposed a bipolar relay coil structure combined with ferrite magnetic circuit optimization techniques [10]. Dong et al. at Wuhan University achieved long-distance constant-current output using multiple coaxially arranged relay coils [11]. Zhao and his team at Xi'an University of Science and Technology applied mutual inductance coupling theory of circuits, combined with axial offset analysis of relay coils, and showed how to attain maximum delivered power and efficiency [12]. However, although long-range WPT is feasible by inserting additional relay stages, each additional coil inevitably introduces eddy current loss, dielectric loss, and skin-effect loss [13], which may result in low system efficiency or even failure to meet practical application requirements. Current research generally explores strategies to enhance the transmission efficiency of WPT systems by investigating coil shapes [14,15], coil geometric parameters [16-19], transmission distance, and coil arrangement methods. Nevertheless, detailed analyses of coil-geometry factors—such as turn count and inner radius, remain limited.

To address the above issues, this paper focuses on the optimal design of coil geometric parameters. Drawing on theory, simulations, and experiments, we propose a joint optimization of the coil inner radius and turn count. The effectiveness of this method in improving transmission efficiency is verified, providing an effective technical approach to tackle the efficiency challenges of long-distance WPT.

2. Model and Principles of Multi-Stage Magnetic Resonant WPT Systems

2.1 System Geometric Model and Equivalent Circuit

The multi-stage resonant WPT system is summarized by its geometry in Fig. 1 and by an equivalent network model in Fig. 2. Here, d_{ij} denotes the axial separation of coil i and coil j, and d denotes the overall Tx-Rx separation. r_j is the inner radius of the coil j, while M_{jk} characterizes the mutual inductance of the (j, k) pair. L_i, R_i, C_i and $\dot{I}_i$ correspond to the self-inductance, internal resistance, compensation capacitance, and complex current phasor of the coil i, respectively (i,

j, k= 1, 2, 3, ···, n-1, n). $\dot{U}_{\mathrm{p}}$ denotes the complex voltage phasor of the transmitting coil, $\dot{U}_{\mathrm{L}}$ the complex load voltage phasor, R_{L} the equivalent load resistance, and ω the angular frequency. All phasors are given in root-mean-square values unless otherwise stated.

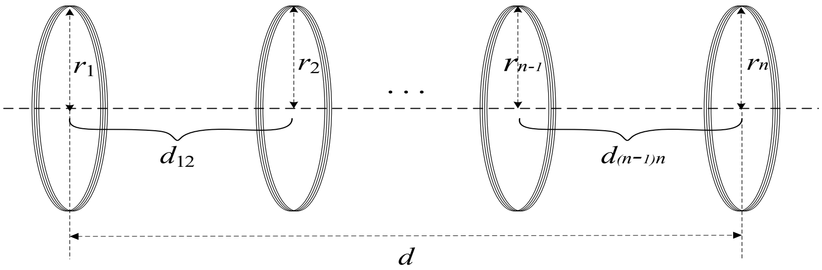

Fig. 1 Geometric parameter model of the multi-coil system

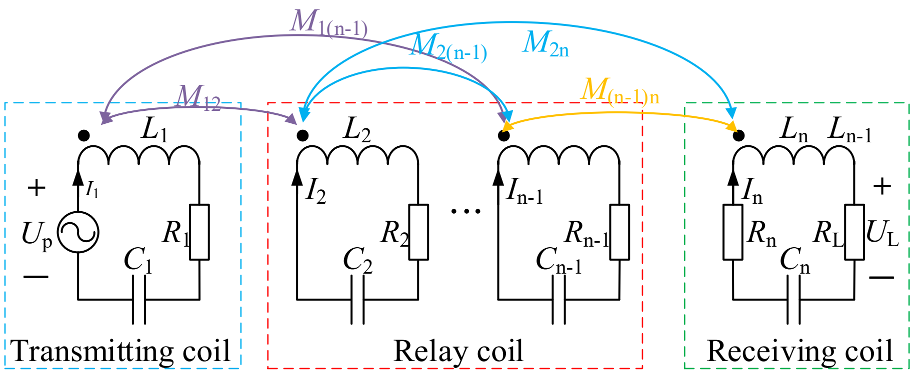

Fig. 2 equivalent network model

2.2 Voltage Equations and Efficiency Modeling

The multi-stage WPT system voltage equations in phasor form can be written as Eq. (1).

$$\begin{cases}\dot{U}_{\mathrm{p}}=\dot{I}_1 R_1+\mathrm{j}\omega M_{12}\dot{I}_2+\ldots+\mathrm{j}\omega M_{1(\mathrm{n}-1)}\dot{I}_{\mathrm{n}-1}+\mathrm{j}\omega M_{1\mathrm{n}}\dot{I}_{\mathrm{n}}\\ 0=\mathrm{j}\omega M_{21}\dot{I}_1+\dot{I}_2 R_2+\ldots+\mathrm{j}\omega M_{2(\mathrm{n}-1)}\dot{I}_{\mathrm{n}-1}+\mathrm{j}\omega M_{2\mathrm{n}}\dot{I}_{\mathrm{n}}\\ \ldots\ldots\\ 0=\mathrm{j}\omega M_{(\mathrm{n}-1)1}\dot{I}_1+\mathrm{j}\omega M_{(\mathrm{n}-1)2}\dot{I}_2+\ldots+\dot{I}_{(\mathrm{n}-1)}R_{(\mathrm{n}-1)}+\mathrm{j}\omega M_{(\mathrm{n}-1)\mathrm{n}}\dot{I}_{\mathrm{n}}\\ 0=\mathrm{j}\omega M_{\mathrm{n}1}\dot{I}_1+\mathrm{j}\omega M_{\mathrm{n}2}\dot{I}_2+\ldots+\mathrm{j}\omega M_{n(\mathrm{n}-1)}\dot{I}_{\mathrm{n}-1}+\dot{I}_{\mathrm{n}}(R_{\mathrm{L}}+R_{\mathrm{n}})\end{cases}\quad(1)$$

The system efficiency is expressed as in Eq. (2).

$$\eta = \frac{P_{\text{out}}}{P_{\text{out}} + P_{\text{loss}}} = \frac{I_{\text{n}}^2 R_{\text{L}}}{U_{\text{p}} I_1} \tag{2}$$

where P_{out} denotes the output power (W), and P_{loss} denotes the losses on all coils (W). Substituting Eq. 1 into the above expression yields Eq. (3).

$$\eta = f(\omega, L_{\text{i}}, C_{\text{i}}, R_i, R_L, M_{\text{ij}})(i, j = 1, 2, 3, \cdots, n) \tag{3}$$

From the expression of mutual inductance for circular coils[20] in Eq. (4), it can be seen that M_{ij} depends not only on the geometric parameters of the coils themselves but also on the coil spacing d_{ij}.

$$\begin{gathered} M_{ij} = N_i N_j \mu_0 \sqrt{r_i r_j} \frac{2}{b} \left[\left(1 - \frac{b^2}{2} \right) \int_0^{\frac{\pi}{2}} \frac{1}{\sqrt{1 - b^2 \sin^2 x}} \mathrm{d}x - \int_0^{\frac{\pi}{2}} \sqrt{1 - b^2 \sin^2 x} \mathrm{d}x \right] \\ b = \sqrt{\frac{4 r_i r_j}{(r_i^2 + r_j^2) + d_{ij}^2}} \end{gathered} \tag{4}$$

where b depends on the structural parameters of the coils, N_i and N_j are the number of turns of the coil i and coil j, r_i and r_j are the inner radii of the coil i and coil j, and $\mu_0 = 4\pi \times 10^{-7}$H/m is the permeability of air.

Since L_i and R_i are functions of the coil inner radius r_i and the turn count N, Eq. (3) can be simplified as follows:

$$\eta = f(\omega, r_i, N_i, d_{ij}, R_L)(i, j = 1, 2, 3, \cdots, n) \tag{5}$$

From Eq. (5), the transmission efficiency strongly depends on the coil turn count and inner radius.

2.3 Modeling and Analysis of a Four-Stage System

In this paper, a four-stage WPT system is taken as an example for formula derivation and simulation analysis. A 3D model of the four-stage magnetically coupled WPT system, as shown in Fig. 3, is established using finite element electromagnetic simulation software, and Baseline geometric settings for the model are given in Table 1.

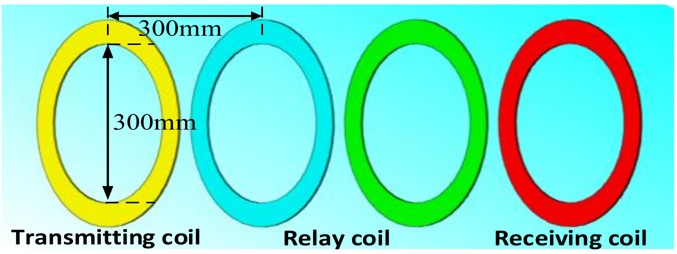

Fig. 3. 3D model of the four-stage magnetic coupler

Table 1

Parameter design of the four-stage magnetic coupler

Coil parameters	Value	System parameters	Value
Coil inner radius *r*/mm	150	Operating frequency *f*/kHz	100
Number of turns *N*	10	Source voltage (rms) U_P/V	50
Wire diamete *a*/mm	3	Load impedance R_L/Ω	5
Coil spacing d_{ij}/mm	300	Coil resistance *R*/Ω	0.5

Since the distances between non-adjacent coils are relatively large, their mutual inductances can be neglected. Meanwhile, the structural parameters and spacing of each stage coil are kept identical, and all coils adopt the fully compensated S-S topology. Under these conditions, the simplified form of Eq. (6) can be obtained. Consequently, the current ratio relationships between each coil and the receiving coil (Eq. (7)), as well as the efficiency expression (Eq. (8)) are derived.

$$\begin{cases} X_1 = X_2 = X_3 = X_4 \\ M_{12} = M_{23} = M_{34} = M \\ R_1 = R_2 = R_3 = R_4 = R \\ d_{12} = d_{23} = d_{34} = d_a \end{cases} \tag{6}$$

$$\begin{bmatrix} \dot{U}_1 \\ 0 \\ 0 \\ 0 \end{bmatrix} = \begin{bmatrix} Z_1 & \mathrm{j}\omega M_{12} & 0 & 0 \\ \mathrm{j}\omega M_{12} & Z_2 & \mathrm{j}\omega M_{23} & 0 \\ 0 & \mathrm{j}\omega M_{23} & Z_3 & \mathrm{j}\omega M_{34} \\ 0 & 0 & \mathrm{j}\omega M_{34} & Z_4 \end{bmatrix} \begin{bmatrix} \dot{I}_1 \\ \dot{I}_2 \\ \dot{I}_3 \\ \dot{I}_4 \end{bmatrix} \tag{7}$$

$$\eta = \frac{I_4^2 R_L}{U_1 I_1} \tag{8}$$

3. Optimization of Coil Geometric Parameters

3.1 Influence of Coil Geometric Parameters on Electrical Characteristics

The geometric structure of a coil is mainly determined by the number of turns and the inner radius, as shown in Fig. 4.

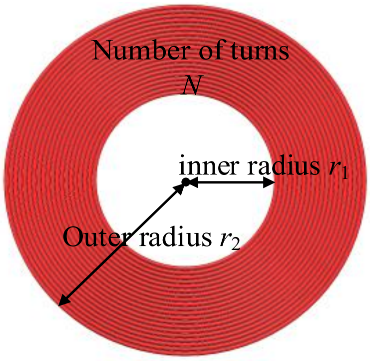

Fig. 4. 3D model of the magnetic flux lines of a single-coil magnetic coupler for theoretical calculation

The DC resistance of the wire can be expressed as:

$$R_{dc} = \frac{\rho l}{A} = \frac{\rho 2\pi r}{A} \tag{9}$$

where ρ is the resistivity of the wire, l is the length of the wire, and A represents the conductor cross-sectional area.

Since the multi-stage WPT system operates under high-frequency conditions, the current distribution is affected by the skin and proximity effect. To mitigate the influence of the skin effect, litz wire composed of multiple fine strands is employed in this study. In this case, the AC resistance can be corrected using the AC resistance factor $F_{r,n}$ [21]:

$$R_{ac} = F_{r,n} R_{dc} \tag{10}$$

where R_{dc} denotes the DC resistance (Ω), and R_{ac} denotes the AC resistance (Ω).

The total resistance of an N-turn coil is given by:

$$R = F_{r,n} \frac{\rho}{A} \sum_{i=1}^{n} l_1 = \frac{2\pi\rho}{A} F_{r,n} (N r_1 + \frac{N(N-1)D}{2}) \tag{11}$$

For a multi-turn coil, the overall self-inductance can be expressed as:

$$L = \frac{\mu_0 N^2 (r_1 + r_2)}{2} \left[\ln \frac{2.46}{\varphi} + 0.2\varphi^2 \right] \tag{12}$$

$$\varphi = \frac{r_2 - r_1}{r_2 + r_1} = \frac{(N-1)D}{2r_1 + (N-1)D} \tag{13}$$

where r_1 denotes the inner radius of the coil, r_2 denotes the outer radius of the coil, N denotes the number of turns of the coil, and D is the wire diameter.

The mutual inductance between two identical circular coils can be obtained using Maxwell's mutual inductance formula:

$$M_{ij} = \frac{\mu_0 \pi r^4 N^2}{2(r^2 + d_{ij}^2)^{3/2}} \tag{14}$$

where r is the average radius of the circular coil.

3.2 Optimization of the Number of Turns

Keeping the inner radius constant, the influence of the number of turns on the system efficiency is analyzed. The approximate relationships of mutual inductance and resistance can be obtained as:

$$M \approx k_1 N^2 \quad R \approx k_2 N \tag{15}$$

where k_1 is the proportional coefficient between mutual inductance and the number of turns, and k_2 is the proportional coefficient between coil resistance and the square of the number of turns. Both k_1 and k_2 are determined by the coil inner radius and the coil spacing. In practical multi-stage WPT systems, the mutual reactance ωM between coils is generally maintained at several to tens of ohms, while the internal resistance of the coils is usually less than 1 Ω, differing by an order of magnitude. By neglecting the higher-order terms of the coil resistance, the simplified system efficiency formula can be obtained:

$$\eta = \frac{R_L}{2k_2 n + \dfrac{2{R_L}^2 k_2}{\omega^2 {k_1}^2 n^3} + \dfrac{4{k_2}^3}{\omega^2 {k_1}^2 n} + R_L} \tag{16}$$

The function curve of efficiency versus turns is overlaid with the numerical results, as illustrated in Fig. 5.

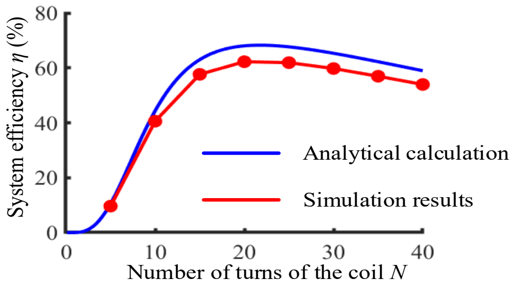

Fig. 5 Effect of coil turns on the transmission efficiency of the system

As shown in Fig. 5, the simulated system efficiency is slightly lower than the analytical result, which is due to the neglect of cross-coupling effects in the formula. However, this does not affect the determination of the optimal number of turns. There exists an optimal number of turns, N_{max}, at which the system efficiency reaches its maximum. To solve for N_{max}, the derivative of the efficiency in Eq. (16) with respect to N is set to zero.

$$\frac{\partial \eta}{\partial N} = 0 \tag{17}$$

From Eq. (17), the expression for the optimal number of turns can be obtained as:

$$N_{\max} = \sqrt{\frac{\frac{4k_2^3}{\omega^2 k_1^2} + \sqrt{(\frac{4k_2^3}{\omega^2 k_1^2})^2 + \frac{48R_L^2 k_2^2}{\omega^2 k_1^2}}}{4k_2}} \tag{18}$$

3.3 Inner radius optimization

Keeping the coil turn count constant, the influence of the inner radius r on efficiency is analyzed. The approximate relationship between efficiency and the coil inner radius can be derived as:

$$\begin{cases} M = f(r) \\ R = k_3 r \end{cases} \tag{19}$$

where k_3 is the proportional coefficient between mutual inductance and the number of turns.

The efficiency formula is obtained as:

$$\eta = \frac{R_L}{2k_3 r + \frac{2R_L^2}{\omega^2 f(r)^2} k_3 r + \frac{4}{\omega^2 f(r)^2}(k_3 r)^3 + R_L} \tag{20}$$

However, the formula of mutual inductance with respect to r is rather complicated and strongly correlated with the coil spacing. Therefore, a simplified fitting method is adopted in this paper, as expressed in Eq. (21):

$$M \approx \begin{cases} A_1 r + B_1 (d_a \in (150mm, 250mm)) \\ A_2 (r + B_2)^2 (d_a \in (250mm, 350mm)) \\ A_3 r^3 (d_a \in (350mm, 450mm)) \end{cases} \tag{21}$$

The approximate expressions of mutual inductance with respect to the inner radius under different coil spacings d_a are compared with the results from the original mutual inductance formula, as shown in Fig. 6. In the figure, the solid lines represent the actual values, while the dashed lines indicate the simplified approximations. It can be observed that the relative error of the simplified method is less than 1% when the coil inner radius is greater than 100 mm.

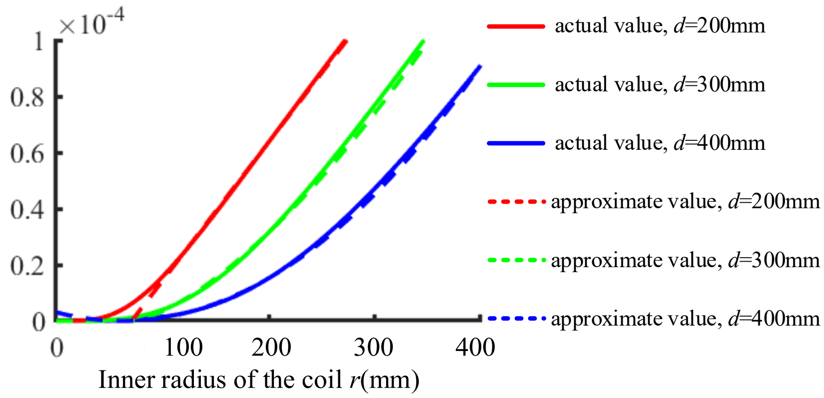

Fig. 6 Variation of coil mutual inductance with r under different spacings before and after simplification

Furthermore, by substituting the simplified formula under the condition of d=300mm into Eq. (20), The efficiency as a function of inner radius is plotted and overlaid with the numerical results, as illustrated in Fig. 7.

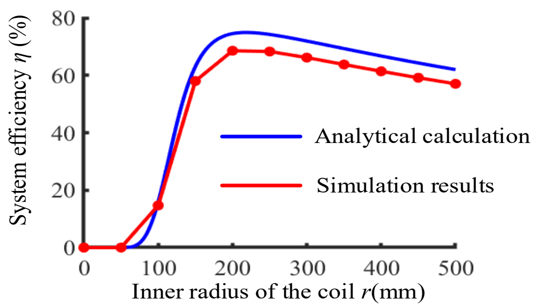

Fig. 7 Influence of coil inner radius on system transmission efficiency

As shown in Fig. 7, the relative error between the simplified formula and the actual efficiency is relatively small. Moreover, the variation of efficiency with respect to the coil inner radius follows the same trend as that with the number of turns. There exists an optimal inner radius r_{max} at which the system efficiency reaches its maximum. To solve for r_{max}, the derivative of the efficiency in Eq. (20) with respect to r is set to zero.

$$\frac{\partial \eta}{\partial r} = 0 \tag{22}$$

Thus, the expression for the optimal number of turns can be obtained as:

$$r_{max} = \left(\frac{5R_L{}^2}{\omega^2 A_2^2}\right)^{\frac{1}{6}} \tag{23}$$

3.4 Joint Optimization of Inner Radius and Number of Turns

From the previous two sections, it is known that the optimal number of turns N_{max} and the optimal inner radius r_{max} influence each other. For a given coil spacing d_a, the two expressions can be combined to obtain the geometric parameters corresponding to the maximum system efficiency:

$$\begin{cases} N_{max} = f_1(r) \\ r_{max} = f_2(N) \end{cases} \tag{24}$$

Taking the four-stage magnetically coupled WPT system with a total transmission distance of 900 mm as an example, the optimal configuration of the geometric parameters of the four-coil system is analyzed. In this case, the coil spacing d_a is 300 mm. By substituting into Eq. (24), the optimal number of coil turns is obtained to be about 5, and the optimal inner radius is about 446 mm. To verify the accuracy of these results, the expressions of coil self-inductance L, resistance R, and mutual inductance M with respect to the geometric parameters N and r, derived in Section 2.1, are substituted into the efficiency formula (Eq. (8)). Accordingly, the efficiency can be represented as a bivariate function depending only on the number of turns and the inner radius. The variation of system efficiency with both coil geometric parameters is shown in Fig. 8.

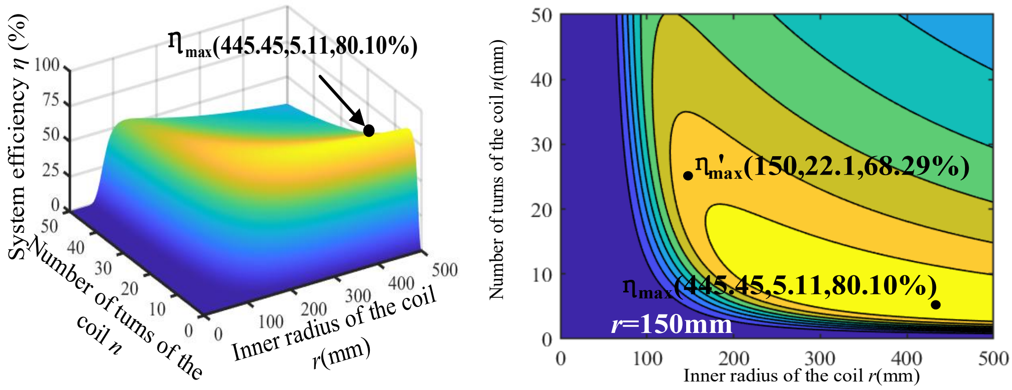

(a)3D diagram (b) 2D contour plot

Fig. 8 Joint influence of coil geometric parameters r and N on system efficiency

From the figure, when the coil inner radius is 445.45 mm and the number of turns is 5.11, the system efficiency reaches the global optimum. At this point, with fewer turns and a larger inner radius, the system efficiency can reach 80.1%.

4. Experimental verification

To assess the effectiveness of the multi-stage resonant WPT geometry co-design proposed in this paper, an experimental platform was built and tested using a four-stage magnetically coupled WPT system as an example. The experimental setup is shown in Fig. 9, and the parameters of the four-stage magnetically coupled WPT system before optimization are listed in Table 2.

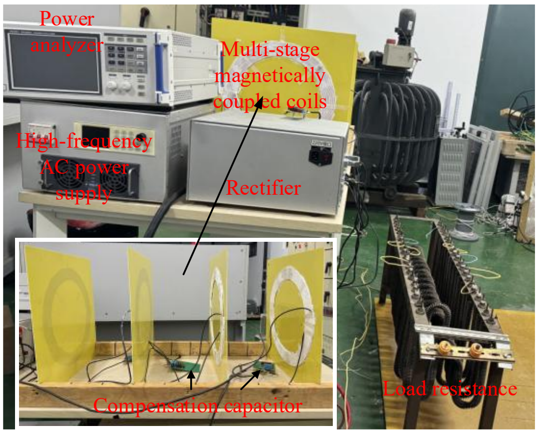

Fig. 9 Experimental platform of the multi-stage magnetic resonant WPT system

Table 2

Coil Parameters before optimization

Coil parameter	Value	Coil parameter	Value
Coil self-inductance L/μH	107.2	Coil internal resistance R/Ω	0.5
Compensation capacitor C/nF	23.61	Operating frequency f/kHz	100
Mutual inductance M/μH	6.92	RMS supply voltage U_p/V	50
Number of turns N	15	Coil inner diameter r/mm	150
Wire diameter a/mm	3	Load resistance R_L/Ω	5
Coil spacing d_{ij}/mm	300	——	——

The validation experiment scheme is shown in the table 3. First, based on the coil inner-radius optimization method and the turn-number optimization method proposed in this paper, the coil parameters for the "inner-radius-only optimization" scheme and the "turn-number-only optimization" scheme are obtained, respectively. Then, using the proposed joint optimization of inner radius and number of turns, the coil parameters after joint optimization are determined. Finally, the system power-transfer efficiency under the baseline scheme and the three optimization schemes is measured and compared. To eliminate the influence of differences in electrical parameters, during the validation of the geometric-parameter optimization methods, all coils are tuned to operate at resonance, the receiver-side load is fixed at 5 Ω, and a constant input voltage of 50 V is applied in the experiment. The experimental results are shown in Table 4.

Table 3

Validation experiment scheme

Experimental scheme	Inner radius r/mm	The number of turns N
Baseline scheme	150	15
Single optimization of inner radius	200	15
Single optimization of the number of turns	150	21
Joint optimization of inner radius and number of turns	445	5

Table 4 presents the experimental results under the different optimization methods described above. The results indicate that adjusting the coil geometry can effectively improve system efficiency. Single-parameter optimization improves the system efficiency by about 3%, while simultaneous optimization of both geometric parameters can further increase the efficiency by 16.9%.

Table 4

Experimental results

Experimental scheme	Efficiency
Baseline scheme	56.809%
Single optimization of inner radius	60.498%
Single optimization of the number of turns	60.087%
Joint optimization of inner radius and number of turns	73.709%

5. Conclusion

This paper addresses the problem of efficiency degradation in multi-stage magnetic resonant WPT systems under medium and long-distance transmission. By establishing a multi-stage WPT model, the relationship between transmission efficiency and coil geometric parameters such as inner radius and number of turns was investigated. A joint optimization method for coil inner radius and number of turns was proposed, which improved the system efficiency by 16.9% after optimization. The results demonstrate that the proposed joint optimization method can significantly enhance the efficiency of multi-stage magnetic resonant WPT systems under medium- and long-distance conditions, providing an effective design approach and reference for practical applications such as online monitoring of transmission lines and power supply of electrical equipment.

Acknowledgment

This work is supported by the R&D project of State Grid Xinjiang Electric Power Co., Ltd. (Research and Application of All-Weather Power Supply Technology for Communication and Monitoring Systems in 10kV Overhead Distribution Lines, No. SGXJXT00JXJS2500097).

REFERENCES

[1]. *N. Tesla*, "Experiments with Alternate Currents of Very High Frequency and their Application to Methods of Artificial Illumination," Transactions of the American Institute of Electrical Engineers, **VIII**, 2007, pp. 266–319.

[2]. *Z. Zhang*, *H. Pang*, *A. Georgiadis*, et al., "Wireless power transfer—An overview," IEEE Transactions on Industrial Electronics, 66(2), 2018, pp. 1044–1058.

[3]. *S. Y. R. Hui*, "Past, present and future trends of non-radiative wireless power transfer," CPSS Transactions on Power Electronics and Applications, **1**(1), 2016, pp. 83–91.

[4]. *A. P. Sample*, *D. T. Meyer*, *J. R. Smith*, "Analysis, experimental results, and range adaptation of magnetically coupled resonators for wireless power transfer," IEEE Transactions on Industrial Electronics, **58**(2), 2010, pp. 544–554.

[5]. *C. Zhu*, *J. Jiang*, *K. Song*, *Q. Zhang*, "Research progress on key technologies of dynamic wireless charging for electric vehicles," Automation of Electric Power Systems, **41**(2), 2017, pp. 1–9.

[6]. *P. Gu*, *D. Yang*, *G. Li*, et al., "Analysis and design of discrete ferrite rings to improve the efficiency of meter-range wireless gap inductive power transfer system," IEEE Transactions on Power Electronics, **38**(10), 2023, pp. 11802–11813.

[7]. *C. Cheng*, *F. Lu*, *Z. Zhou*, et al., "Load-independent wireless power transfer system for multiple loads over a long distance," IEEE Transactions on Power Electronics, **34**(9), 2018, pp. 9279–9288.

[8]. *D. E. Gaona*, *C. Jiang*, and *T. Long*, "Highly efficient 11.1-kW wireless power transfer utilizing nanocrystalline ribbon cores," IEEE Transactions on Power Electronics, **36**(9), 2021, pp. 9955–9969.

[9]. *W. Wang*, *Z. Zeng*, *J. Wang*, "Performance analysis and optimization of non-uniform domino unit in wireless power supply system of transmission tower," Transactions of China Electrotechnical Society, **37**(17), 2022, pp. 4316–4325.

[10]. *C. Cheng*, *F. Lu*, *Z. Zhou*, et al., "Load-independent wireless power transfer system for multiple loads over a long distance," IEEE Transactions on Power Electronics, **34**(9), 2018, pp. 9279–9288.

[11]. *Z. Dong*, *S. Liu*, *X. Li*, et al., "A novel long-distance wireless power transfer system with constant current output based on domino-resonator," IEEE Journal of Emerging and Selected Topics in Power Electronics, **9**(2), 2020, pp. 2343–2355.

[12]. *Y. Zhao*, *G. Wan*, *Y. Wang*, "Optimization research on the axial position of the relay coil in the three-coil MCR-WPT system," Electronic Measurement Technology, **46**(4), 2023, pp. 1–5.

[13]. *S. Y. R. Hui*, *W. W. C. Ho*, "A new generation of universal contactless battery charging platform for portable consumer electronic equipment," IEEE Transactions on Power Electronics, **20**(3), 2005, pp. 620–627.

[14]. *P. Tan*, *B. Song*, *X. Shangguan*, et al., "Optimal design of transmission characteristics for hexagonal coil wireless power transfer system based on genetic algorithm," Chinese Journal of Electrical Engineering, **9**(2), 2023, pp. 94–106.

[15]. *M. Budhia*, *J. T. Boys*, *G. A. Covic*, et al., "Development of a single-sided flux magnetic coupler for electric vehicle IPT charging systems," IEEE Transactions on Industrial Electronics, **60**(1), 2011, pp. 318–328.

[16]. *S. Y. Choi*, *J. Huh*, *W. Y. Lee*, et al., "Asymmetric coil sets for wireless stationary EV chargers with large lateral tolerance by dominant field analysis," IEEE Transactions on Power Electronics, **29**(12), 2014, pp. 6406–6420.

[17]. *F. Wen*, *X. Chu*, *Q. Li*, et al., "Optimization on three-coil long-range and dimension-asymmetric wireless power transfer system," IEEE Transactions on Electromagnetic Compatibility, **62**(5), 2020, pp. 1859–1868.

[18]. *Z. Yuan*, *X. Zhang*, *Q. Yang*, "Asymmetric coupling mechanism of wireless power transmission system for high-speed train," Transactions of China Electrotechnical Society, **32**(18), 2017, pp. 19–25.

[19]. *Y. Li*, *J. Yin*, *Q. Yang*, et al., "Influence of internal resistance and quality factor of asymmetric coupled coils on transmission power, efficiency, and frequency splitting," Transactions of China Electrotechnical Society, **33**(12), 2018, pp. 2743–2750.

[20]. *C. K. Lee*, *W. X. Zhong*, *S. Y. R. Hui*, "Effects of magnetic coupling of nonadjacent resonators on wireless power domino-resonator systems," IEEE Transactions on Power Electronics, **27**(4), 2011, pp. 1905–1916.

[21]. *K. Zhang*, *X. Cao*, *G. Qiao*, "Analysis of winding loss calculation methods for high-frequency transformers," Proceedings of the CSEE, **39**(18), 2019, pp. 5536–5546.